

Production of $\psi(2S) \rightarrow \psi + J/\psi$

M. Ablikim¹, J. Z. Bai¹, Y. Ban¹², X. Cai¹, H. F. Chen¹⁷, H. S. Chen¹, H. X. Chen¹, J. C. Chen¹, Jin Chen¹, Y. B. Chen¹, S. P. Chi², Y. P. Chu¹, X. Z. Cui¹, Y. S. Dai⁹, L. Y. Diao⁹, Z. Y. Deng¹, Q. F. Dong¹⁵, S. X. Du¹, J. Fang¹, S. S. Fang², C. D. Fu¹, C. S. Gao¹, Y. N. Gao¹⁵, S. D. Gu¹, Y. T. Gu⁴, Y. N. Guo¹, Y. Q. Guo¹, Z. J. Guo¹⁶, F. A. Harris¹⁶, K. L. He¹, M. He¹³, Y. K. Heng¹, H. M. Hu¹, T. Hu¹, G. S. Huang^{1a}, X. T. Huang¹³, X. B. Ji¹, X. S. Jiang¹, X. Y. Jiang⁵, J. B. Jiao¹³, D. P. Jin¹, S. Jin¹, Yi Jin⁸, Y. F. Lai¹, G. Li², H. B. Li¹, H. H. Li¹, J. Li¹, R. Y. Li¹, S. M. Li¹, W. D. Li¹, W. G. Li¹, X. L. Li¹, X. N. Li¹, X. Q. Li¹¹, Y. L. Li⁴, Y. F. Liang¹⁴, H. B. Liao¹, B. J. Liu¹, C. X. Liu¹, F. Liu⁶, Fang Liu¹, H. H. Liu¹, H. M. Liu¹, J. Liu¹², J. B. Liu¹, J. P. Liu¹⁸, Q. Liu¹, R. G. Liu¹, Z. A. Liu¹, Y. C. Lou⁵, F. Lu¹, G. R. Lu⁵, J. G. Lu¹, C. L. Luo¹⁰, F. C. Ma⁹, H. L. Ma¹, L. L. Ma¹, Q. M. Ma¹, X. B. Ma⁵, Z. P. Ma¹, X. H. Mo¹, J. N. Nie¹, S. L. Olsen¹⁶, H. P. Peng^{17d}, R. G. Ping¹, N. D. Qian¹, H. Qian¹, J. F. Qiu¹, Z. Y. Ren¹, G. Rong¹, L. Y. Shan¹, L. Shang¹, C. P. Shen¹, D. L. Shen¹, X. Y. Shen¹, H. Y. Sheng¹, H. S. Sun¹, J. F. Sun¹, S. S. Sun¹, Y. Z. Sun¹, Z. J. Sun¹, Z. Q. Tan⁴, X. Tang¹, G. L. Tong¹, G. S. Vamer¹⁶, D. Y. Wang¹, L. Wang¹, L. L. Wang¹, L. S. Wang¹, M. Wang¹, P. Wang¹, P. L. Wang¹, W. F. Wang^{1b}, Y. F. Wang¹, Z. Wang¹, Z. Y. Wang¹, Zhe Wang¹, Zheng Wang², C. L. Wei¹, D. H. Wei¹, N. Wu¹, X. M. Xia¹, X. X. Xia¹, G. F. Xu¹, X. P. Xu⁶, Y. Xu¹¹, M. L. Yan¹⁷, H. X. Yang¹, Y. X. Yang³, M. H. Ye², Y. X. Ye¹⁷, Z. Y. Yi¹, G. W. Yu¹, C. Z. Yuan¹, J. M. Yuan¹, Y. Yuan¹, S. L. Zang¹, Y. Zeng⁷, Yu Zeng¹, B. X. Zhang¹, B. Y. Zhang¹, C. C. Zhang¹, D. H. Zhang¹, H. Q. Zhang¹, H. Y. Zhang¹, J. W. Zhang¹, J. Y. Zhang¹, S. H. Zhang¹, X. M. Zhang¹, X. Y. Zhang¹³, Yi Yun Zhang¹⁴, Z. P. Zhang¹⁷, D. X. Zhao¹, J. W. Zhao¹, M. G. Zhao¹, P. P. Zhao¹, W. R. Zhao¹, Z. G. Zhao^{1c}, H. Q. Zheng¹², J. P. Zheng¹, Z. P. Zheng¹, L. Zhou¹, N. F. Zhou^{1c}, K. J. Zhu¹, Q. M. Zhu¹, Y. C. Zhu¹, Y. S. Zhu¹, Yingchun Zhu^{1d}, Z. A. Zhu¹, B. A. Zhuang¹, X. A. Zhuang¹, B. S. Zou¹

(BES Collaboration)

¹ Institute of High Energy Physics, Beijing 100049, People's Republic of China² China Center for Advanced Science and Technology (CAST), Beijing 100080, People's Republic of China³ Guangxi Normal University, Guilin 541004, People's Republic of China⁴ Guangxi University, Nanning 530004, People's Republic of China⁵ Henan Normal University, Xinxiang 453002, People's Republic of China⁶ Huazhong Normal University, Wuhan 430079, People's Republic of China⁷ Hunan University, Changsha 410082, People's Republic of China⁸ Jinan University, Jinan 250022, People's Republic of China⁹ Liaoning University, Shenyang 110036, People's Republic of China¹⁰ Nanjing Normal University, Nanjing 210097, People's Republic of China¹¹ Nankai University, Tianjin 300071, People's Republic of China¹² Peking University, Beijing 100871, People's Republic of China¹³ Shandong University, Jinan 250100, People's Republic of China¹⁴ Sichuan University, Chengdu 610064, People's Republic of China¹⁵ Tsinghua University, Beijing 100084, People's Republic of China¹⁶ University of Hawaii, Honolulu, HI 96822, USA¹⁷ University of Science and Technology of China, Hefei 230026, People's Republic of China¹⁸ Wuhan University, Wuhan 430072, People's Republic of China¹⁹ Zhejiang University, Hangzhou 310028, People's Republic of China^a Current address: Purdue University, West Lafayette, IN 47907, USA^b Current address: Laboratoire de l'Accélérateur Linéaire, Orsay, F-91898, France^c Current address: University of Michigan, Ann Arbor, MI 48109, USA^d Current address: DESY, D-22607, Hamburg, Germany

Using 14M $\psi(2S)$ events accumulated by BESII at the BEPC, a Covariant Helicity Amplitude Analysis is performed for $\psi(2S) \rightarrow \psi + J/\psi$; $J/\psi \rightarrow \psi + \psi$. The ψ mass spectrum, distinctly different from phase space, suggests production in this process. Two different theoretical schemes are used in the global fit to the data. The results are consistent with the existence of the $\psi(2S)$. The pole position is determined to be $\sqrt{s} = 3696.84 \pm 0.12 \pm 0.11$ MeV.

1. Introduction

We report here a study of the process $(2S) \rho^+ \pi^+ J/\psi$, which is the $(2S)$ decay mode with the largest branching fraction [1], using very clean $(2S) \rho^+ \pi^+ J/\psi$ ($J/\psi \rightarrow \mu^+ \mu^-$) events. Early investigations of this decay by Mark I [2] found that the ρ^+ mass distribution is strongly peaked toward higher mass in contrast to what is expected from phase space. Furthermore, angular distributions favored S-wave production between the ρ^+ system and J/ψ , as well as an S-wave decay of the dipion system.

BES I studied this process with much higher statistics (3.8 million $(2S)$ events) and found that an additional small D-wave component was required in the decay of the dipion system [3]. Also various heavy quarkonium models were tested, and the parameters for these models determined [3].

Here, we test the ρ^+ system from $(2S) \rho^+ \pi^+ J/\psi$ decays with the $J^{PC} = 0^{++}$ meson. In this decay, the interaction between the ρ^+ system and $(2S)$ or J/ψ is small since these charmonium states are very narrow, so the dipion system is a quasi-isolated system [4].

The ρ meson was introduced theoretically in the linear model [5], and its existence was first suggested in a one-boson-exchange potential model of nuclear forces [6]. The ρ meson is important due to its relation with dynamical chiral symmetry breaking of QCD [7].

There was evidence for a low mass pole in early DM2 [8] and BES I [9] data on $J/\psi \rightarrow \rho^+ \pi^+$. A huge event concentration in the $I = 0$ S-wave channel was observed in a pp central production experiment in the region from $m = 500$ to $600 \text{ MeV}/c^2$ [10]. This peak is too large to be explained as background [11]. Many studies on the possible resonance structure in scattering have appeared in the literature [12]. It was proved that the existence of a light and broad resonance is unavoidable even with non-linear realization of chiral symmetry [13]. Careful theoretical analyses were made to determine the pole location, which was found to be $M_{\rho(12)} = (470 \pm 30) - i(295 \pm 20) \text{ MeV}/c^2$ [14] and $M_{\rho(12)} = (470 \pm 50) - i(285 \pm 25) \text{ MeV}/c^2$ [15].

Renewed experimental interest arose from E791 data on $D^+ \rightarrow \rho^+ \pi^+$ [16], where it was found that $M_{\rho(12)} = 478^{+24}_{-23} - i(17 \pm 1) \text{ MeV}/c^2$, $\Gamma_{\rho(12)} = 324^{+42}_{-40} - i(21 \pm 2) \text{ MeV}/c^2$. In the recent partial wave analysis of the decay $J/\psi \rightarrow \rho^+ \pi^+$ [17] by BES II, the pole position of $\rho(12)$ was determined to be $(541 \pm 39) - i(252 \pm 42) \text{ MeV}/c^2$. All these experimental results still have large uncertainties.

Fig. 1 shows the decay mechanism of $(2S) \rho^+ \pi^+ J/\psi$ in the S-matrix formalism. There are three main contributions including an S-wave resonance ($\rho(12)$), a D-wave term ($\rho(2^+)$), and a contact term which is the destructive background required by chiral symmetry [18]. The total amplitude is the sum of these three components. The decay $(2S) \rho^+ \pi^+ J/\psi$ can also be described with an effective Lagrangian for the vector pseudo-scalar pseudo-scalar (VPP) vertex, along with the final state interaction (FSI) obtained from scattering data in a Chiral Unitary Approach (ChUA) [19]. In such an approach, the $\rho(12)$ resonance is generated dynamically as a pole of the unitarized t-matrix, and the pole position is $469 - i(203 \pm 2) \text{ MeV}/c^2$ [20]. As to the BES I $(2S) \rho^+ \pi^+ J/\psi$ data shows that the FSI plays an important role in this process [19]. A similar result was obtained in Ref. [21] with a comparison of the cases with and without the FSI. We test our data with both the S-matrix and ChUA schemes.

2. BES II Experiment

The data sample used for this analysis is taken with the BES II detector at the BEPC storage ring operating at the $(2S)$ resonance. The number of $(2S)$ events is 14.0 ± 0.6 million [22], determined from the number of inclusive hadrons.

The Beijing Spectrometer (BES) detector is a conventional solenoidal magnet detector that is described in detail in Ref. [23]; BES II is the upgraded version of the BES detector [24]. A 12-layer vertex chamber (VC) surrounding the beam pipe provides track and trigger information. A 40-layer main drift chamber (MDC), located radially outside the VC, provides trajectory and energy loss (dE/dx) information for charged tracks over 85% of the total solid angle. The mo-

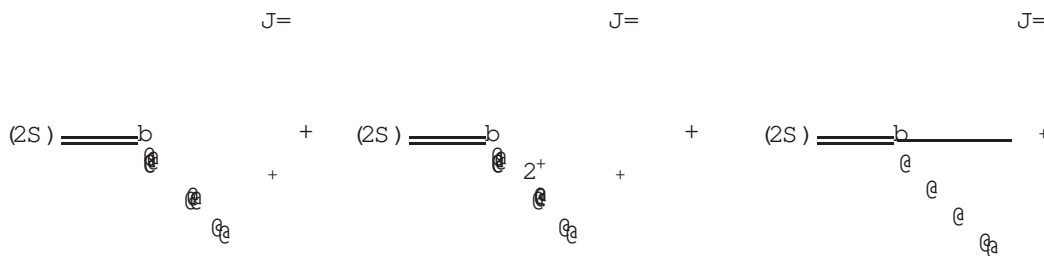


Figure 1. Decay mechanisms for $(2S) \rightarrow J=0$ in the S-matrix formalism. The final amplitude is the superposition of $(2S) \rightarrow J=0$, $(2S) \rightarrow 2^+ J=0$, and $(2S) \rightarrow (1^+)_{\text{cont}} J=0$ S-matrix elements.

momentum resolution is $\frac{\Delta p}{p} = 0.017 \sqrt{1+p^2}$ (p in GeV/c), and the dE/dx resolution is 8%. An array of 48 scintillation counters surrounding the MDC measures the time-of-flight (TOF) of charged tracks with a resolution of 200 ps for hadrons. Radially outside the TOF system is a 12 radiation length, lead-gas barrel shower counter (BSC). This measures the energies of electrons and photons over 80% of the total solid angle with an energy resolution of $\frac{\Delta E}{E} = 22\% = \frac{\Delta E}{E}$ (E in GeV). Outside the solenoidal coil, which provides a 0.4 Tesla magnetic field over the tracking volume, is an iron flux return that is instrumented with three double layers of counters (MUID) that identify muons of momentum greater than 0.5 GeV/c.

A GEANT3 based Monte Carlo (MC) simulation program [25] with detailed consideration of detector performance (such as dead electronic channels) is used to simulate the BESII detector. The consistency between data and MC simulation has been carefully checked in many high purity physics channels, and the agreement is quite reasonable [25].

3. Event Selection

Events with $\psi(3770)$ final states and with the invariant mass $m_{\psi(3770)}$ constrained to the $J=0$ mass are selected for analysis. Each track, reconstructed using hits in the MDC, must have a good helix fit in order to ensure a correct error matrix

in the kinematic fit, and the number of tracks are required to be between 4 and 7.

To select a pair of muons, the muon pair candidates tracks are required to have net charge zero; $p_{\psi(3770)} > 1.3$ GeV/c or $p_{\psi(3770)} > 1.3$ GeV/c or $p_{\psi(3770)} + p_{\psi(3770)} > 2.4$ GeV/c; $|\cos \theta| < 0.6$ to ensure that tracks are in the sensitive region of the MUID; the cosine of the angle between these two tracks in their rest frame $\cos \theta_{\text{cm}} < 0.975$ to guarantee the collinearity of the tracks; the sum of the MUID hits $N_{\text{hit}}^+ + N_{\text{hit}}^- \geq 3$ to ensure that the tracks are muons; and the invariant mass of two candidate tracks $m_{\mu\mu}$ within 0.35 GeV/ c^2 of the $J=0$ mass.

For $\psi(3770)$ pair selection, the two candidate tracks are also required to have net charge zero. Each track is required to have momentum $p < 0.5$ GeV/c, polar angle $|\cos \theta| < 0.75$, and transverse momentum $p_{xy} > 0.1$ GeV/c to reject tracks that spiral in the MDC. The dE/dx measurement of each track must be within three standard deviations of the dE/dx expected for the pion hypothesis, and the cosine of the laboratory angle between the candidate tracks must satisfy $\cos \theta < 0.9$ to eliminate e^+e^- pairs from conversions. The mass recoiling against the candidate $\psi(3770)$ pair, m_{recoil}^+ , is shown in Fig. 2a. In order to get well reconstructed signal events and to suppress background, $|m_{\text{recoil}}^+ - m_{J=0}| < 20$ MeV/ c^2 , corresponding to three times the mass resolution, is required.

With the above selection criteria, about 40,000 $(2S) \rightarrow \pi^+ J/\psi \rightarrow \pi^+ \pi^+ \pi^-$ candidate events are obtained. Fig. 2b shows the π^+ invariant mass distribution for these events, where the dots with error bars are data, and the histogram is Monte Carlo simulation with the PPGEN generator, which is based on chiral symmetry arguments and partially conserved axial vector currents [26]. It describes the low mass spectrum reasonably well but not the high mass region; the inconsistency between data and Monte Carlo will be considered in the systematic errors.

The main background channels are $(2S) \rightarrow J/\psi (J/\psi \rightarrow \pi^+ \pi^-)$, $(2S) \rightarrow \pi^+ J/\psi (J/\psi \rightarrow \pi^+ \pi^-)$ and $(2S) \rightarrow \pi^+ J/\psi (J/\psi \rightarrow \pi^0 \pi^0)$. However, MC simulation indicates that their total contribution is less than 0.1%, which can be neglected. The contamination from continuum production $e^+e^- \rightarrow \pi^+ \pi^-$ is also very small and neglected in this analysis.

4. Analysis Method

Two different schemes are used to fit our data. In the first, based on the diagrams in Fig. 1 and taking the VPP vertex as a constant, the total differential cross section which describes $(2S) \rightarrow \pi^+ J/\psi$ is

$$\frac{d}{d} = \sum_M \int \mathcal{A}^2$$

$$= \sum_M A_0 + \sum_2 A_2 + A_{\text{contact}}; \quad (1)$$

where A_s represents the amplitude for $(2S) \rightarrow X J/\psi \rightarrow \pi^+ J/\psi$ with the spin of X being s , \int represents the solid angle, M is the magnetic quantum number along Z -axis of $(2S)$, and $_2$ are the helicities of the J/ψ and 2^+ components, respectively, and A_{contact} is the amplitude of the contact term.

In the second, considering the VPP vertex and the S-wave FSI, while neglecting the D-wave FSI, the amplitude is [19]

$$A = V_0 + V_{0S} G \frac{I_{\pi_1^0}}{2t_1^0}; \quad (2)$$

$$V_0 = \frac{4}{f^2} (g_1 p_1 \cdot p + g_2 p_1^0 p_2^0 + g_3 m^2) \quad (3)$$

where G is the two-pion loop propagator, V_{0S} is the S-wave part of V_0 , and $t^{I=0}$ is the full S-wave $I=0$ $\pi\pi$ matrix, which is the same as those defined in Refs. [19,20]; p and p_2 are the four momenta of the two pions, and p_1^0 and p_2^0 are their energies in the lab frame; g_1, g_2 , and g_3 are free parameters to be determined by data.

The normalized probability density function used to describe the whole decay process is

$$f(x; \theta) = \frac{d}{d}; \quad (4)$$

where x represents a set of quantities which are measured by experiment, and θ represents unknown parameters to be determined. The total cross section, σ , can be expressed as

$$\sigma = \int \epsilon(x) \frac{d}{d}; \quad (5)$$

where $\epsilon(x)$ is the detection efficiency which is usually a function of detector performance. The total cross section can be determined by MC integration. Re-weighting a total of N generated events based on simulated $(2S) \rightarrow \pi^+ J/\psi$ using a phase space generator, the total cross section is then

$$\sigma = \frac{1}{N_{\text{MC}}} \sum_{i=1}^{N_{\text{MC}}} \frac{d}{d}_i; \quad (6)$$

where $N_{\text{MC}} (< N)$ is the number of MC simulated events after applying the selection criteria.

The maximum likelihood function [27,28] is given by the joint probability density of the selected $(2S) \rightarrow \pi^+ \pi^+ \pi^-$ events,

$$L = \prod_{i=1}^{N_{\text{Evt}}} f(x_i; \theta); \quad (7)$$

and a set of values, θ , is obtained by minimizing the function S ,

$$S = -\log L; \quad (8)$$

For the amplitudes in the first model, the amplitudes for the cascade two-body decay process can be expanded with helicity amplitudes as:

$$A_s = F^J D_M^J; \quad BW_X(S; m_X; x) F_{00}^S D_{s;0}^S; \quad (9)$$

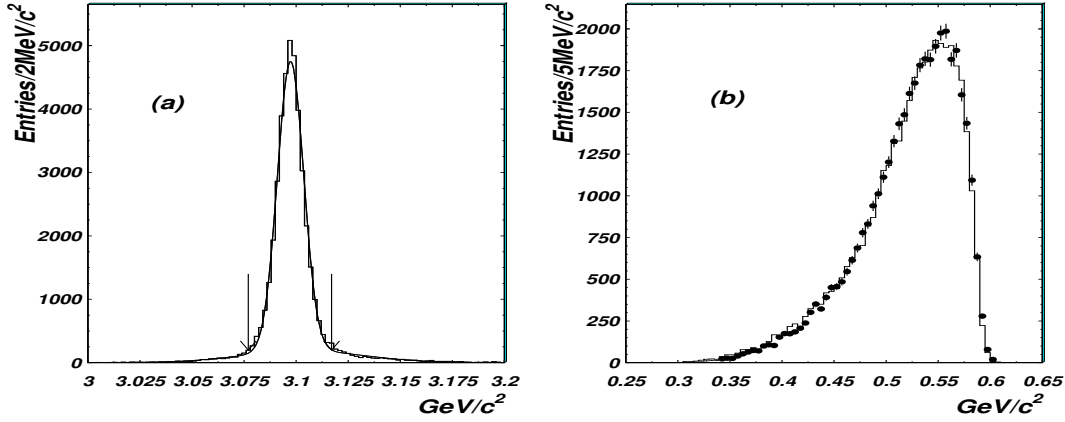


Figure 2. Distributions of candidate $(2S) J=0$ events. (a) is the $(2S) J=0$ recoil mass spectrum, fitted with a double Gaussian function, and (b) is the $(2S) J=0$ invariant mass spectrum. The histogram in (a) is data, the curve is the fit, the events between arrows are selected; in (b) dots with error bars are data, and the histogram is MC simulation.

where F^J is the helicity amplitude, which can be found in Ref. [28], $D_M^J(s; m_X; 0)$ is the D -function, and $BW_X(s; m_X; \Gamma_X)$ is the Breit-Wigner propagator of X , defined as:

$$BW_X(s; m_X; \Gamma_X) = \frac{1}{s - m_X^2 + im_X \Gamma_X(s)} \quad (10)$$

The $(2S) J=0$ particle, a broad structure in the low $(2S) J=0$ mass region, is not a typical Breit-Wigner resonance. In the first model, four types of Breit-Wigner parameterizations are used to describe it:

1) Constant width

$$x(s) = \frac{r}{m_X^2 - s} \quad (11)$$

2) Width containing a kinematic factor, which was used by the E791 Collaboration [16]

$$x(s) = \frac{r}{m_X^2 - s} \frac{4m_X^2}{s} \quad (12)$$

3) P K J ansatz [29], which removes the spurious singularity hidden in Eq. (12)

$$x(s) = \frac{s}{m_X^2} \frac{r}{1 - \frac{4m_X^2}{s} \frac{s}{m_X^2}} \quad (13)$$

4) Zou and Bugg's approach [30], where the form includes explicitly into $x(s)$ the Adler zero at $s = m^2 = 2$.

$$x(s) = g_1 \frac{(s)}{(m_X^2 - s)} + g_2 \frac{4(s)}{4(m_X^2 - s)} \quad (14)$$

$$g_1 = f(s) \frac{s - m^2 = 2}{m_X^2 - m^2 = 2} e^{-\frac{s - m_X^2}{a}};$$

where the definitions of r , a , and $f(s)$ are the same as Ref. [17].

5. Partial wave analysis

The minimization used in the partial wave analysis and to obtain the pole parameters of the (0^+) is based on MINUIT [31]. For the first model, the components considered include amplitudes of (0^+) , a D -wave term, and a contact term. The

tail of the $f_0(980)$ has been tried in the fit. However, it has similar behavior to the contact term in this mass region, and therefore it is ascribed to the contact term. All four Breit-Wigner parameterizations fit the data well, but have strong destructive interference with the contact term, especially in the low \sqrt{s} invariant mass region. The D-wave contribution is only 0.3 to 1%, in agreement with the BES1 result [3] based on a different analysis method. Fig. 3 shows the projections of the fit results compared with data for the Breit-Wigner parameterization for the PKJ ansatz; other parameterizations give similar results.

The global fits determine the best estimation of the Breit-Wigner parameters for each parameterization. The pole position in the complex energy plane is related to the mass and width of the resonance by

$$P_{\text{pole}} = m - i\frac{\Gamma}{2} \quad (15)$$

The best fit results and the corresponding pole positions for all the parameterizations are listed in Table 1. The statistical error of the resonance mass (width) is determined by a decrease of $\frac{1}{2}$ in the log-likelihood from its maximum value with all other parameters fixed to their best solutions.

For the second model, where the VPP vertex is represented by an effective Lagrangian and the S-wave FSI is included, the mass spectrum can also be reproduced well. Here the fit requires a much smaller interference between the S-wave FSI and the contact term. In this case, the fit is worse than the fits of the first model; this may be due to the fixed pole position of the ρ and the neglected D-wave contribution. For the second model, the pole is not measured in the fit, but taken from Ref. [20], which was determined from scattering data.

To check the goodness of fit in our analysis, we construct a variable

$$\chi^2_{\text{obs}} = \sum_{i=1}^N \frac{N_i^{\text{D T}} - N_i^{\text{M C}}}{N_i^{\text{D T}}} \quad ; \quad (16)$$

where N is the number of cells, $N_i^{\text{D T}}$ and $N_i^{\text{M C}}$ are the numbers of events in the i 'th cell of the

Dalitz plot with axes $m^2_{\pi^+}$ and $m^2_{\pi^+ \pi^-}$ for data and MC simulation, respectively. Such a variable should be distributed according to the χ^2 distribution with $n = N - K$ degrees of freedom, where $K = 12$ is the number of parameters to be determined in our Maximum Likelihood fit. In our case, 15 bins in both $m^2_{\pi^+}$ and $m^2_{\pi^+ \pi^-}$ give 225 cells. To ensure proper $\chi^2(n)$ behavior, cells with less than five events have been merged into adjacent ones. The number of cells becomes $N = 208$, and the number of degrees of freedom $n = 196$. From the observed χ^2 value determined using Eq. (16) for each parameterization, the confidence levels (C.L.) are calculated and listed in Table 1.

6. Systematic Errors

For the first model, the systematic error of the pole position arises from the uncertainties of the strength of the 2^+ component, the form of the contact term, and the inconsistency between data and of MC simulation. For the 2^+ component, we conservatively remove it from the fit, and the difference of the fitted values from the nominal values are taken as systematic errors. Two contact terms, namely, constant amplitude and $\alpha_1 + i\alpha_2$, where α_1 and α_2 are two parameters to be fitted, are adopted in the fit; the difference is considered as the systematic error. The MC simulation and data have different mass resolutions in the high mass region of the $\pi^+ \pi^-$ system. A modification of π^+ mass resolution is made to improve the fit, and the difference of the fitted pole positions with and without this modification is taken as the systematic error. The systematic error from non-signal backgrounds is neglected.

In order to obtain the mass and $\frac{\Gamma}{2}$ errors in Eq. (15), we set the denominator in Eq. (10) equal to zero and obtain the pole position and corresponding errors by taking into account the mass and width errors of the Breit-Wigner parameterizations. This is done using a MC sampling method, where the correlation between the mass and width is ignored. Table 2 summarizes the systematic errors from all sources, and Table 1 lists the parameters of pole position and their total errors.

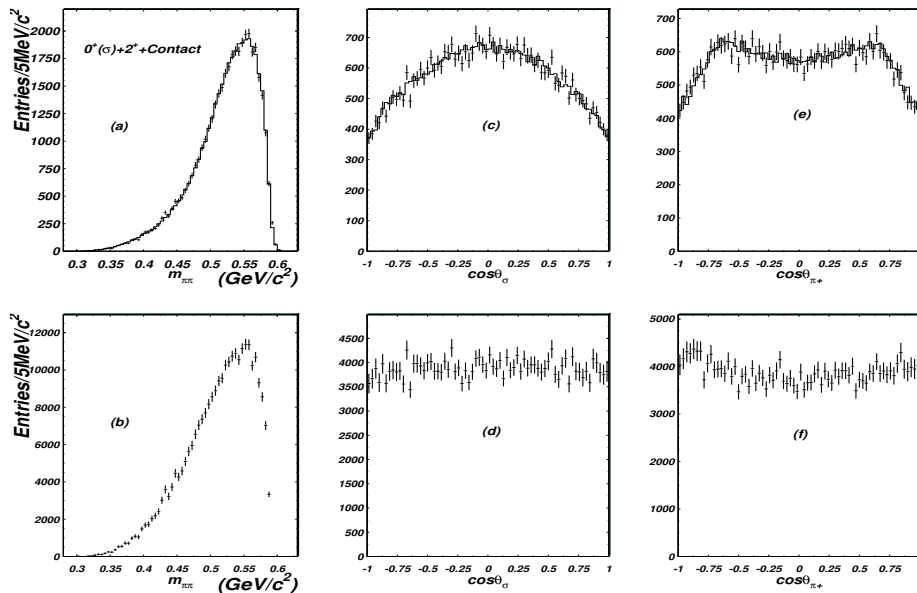


Figure 3. Fit results of $(2S) \rightarrow \pi^+ \pi^-$ with $J = 0^+$ (P-K-J ansatz). Dots with error bars are data and the histograms are the fit results. (a) and (b) are the $\pi^+ \pi^-$ invariant mass, (c) and (d) the cosine of the polar angle in the lab frame, and (e) and (f) the cosine of the π^+ polar angle in the rest frame. The upper plots are the detected distributions, while the bottom ones are the distributions after efficiency correction.

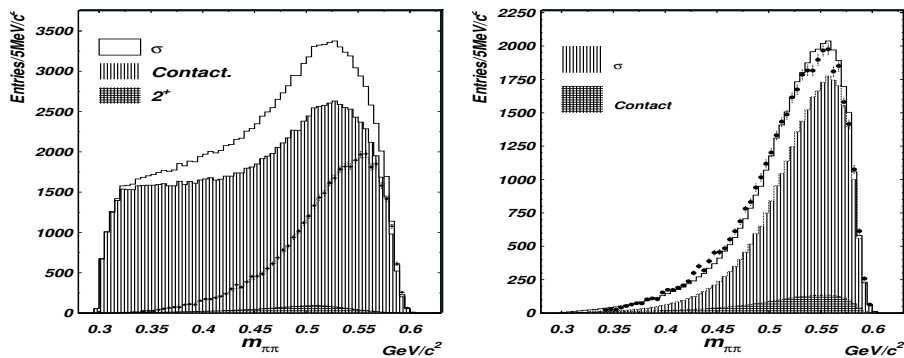


Figure 4. The $\pi^+ \pi^-$ invariant mass distribution including the components. The left is the P-K-J ansatz, which has the contributions from σ , D-wave term, contact term, and their sum (the D-wave is enlarged by a factor of 20 in the figure). The right is the $\pi^+ \pi^-$ invariant mass fitted by the formula from Ref. [19,20], with no explicit D-wave. Dots with error bars are data, and the histograms are the fit results.

Table 1
Fit results of the two models and all the Breit-Wigner parameterizations

Model	Constant	with	P.K.U. ansatz	Bugg & Zou's approach	Ref. [19,20]
Pole (M eV/ c^2)	(553 15 47)	(559 6 26)	(554 13 65)	(541 9 95)	469 i203
N_{γ}	i(254 23 54)	i(179 7 18)	i(240 4 19)	i(253 8 33)	(input)
N_{contact}	140308	72735	133208	171586	30765
$-\ln L$	121625	63133	111230	157741	3039
$-\ln L$	-16174.5	-16166.8	-16171.0	-16174.3	-15974.1
$\chi^2_{\text{obs}}/\text{ndf}$	217.83/196	227.54/196	224.07/196	217.88/196	392.73/208
C.L.	0.1362	0.0608	0.0825	0.1357	3 10 ⁻¹³

N_{γ} and N_{contact} are the numbers of events in the fit.

Table 2
Systematic errors in the pole position (M eV/ c^2)

	Constant		with		P.K.U. ansatz		Bugg & Zou's approach	
	m	=2	m	=2	m	=2	m	=2
2^+ uncertainty	22	35	4	14	10	2	3	3
form of contact term	11	14	1	2	30	8	91	22
M.C. in perfection	40	38	25	10	56	17	37	24
Total Error	47	54	26	18	65	19	95	33

7. Results and discussion

The process $(2S) \rightarrow \pi^+ J/\psi; J/\psi \rightarrow \pi^+ \pi^-$ is studied based on $14 \cdot 10^6$ $(2S)$ events collected with the BESII detector. The π^+ invariant mass spectrum of $(2S) \rightarrow \pi^+ J/\psi$ has a severe suppression near the π^+ threshold, which is distinctly different from phase space and suggests ρ production in the process. We fit the data with two different models. For the first model, using four different Breit-Wigner parameterizations, the data can be well fitted, although a strong cancellation between the ρ and the contact term is required. In fact, such a large cancellation is dictated by chiral symmetry [26,18]. The pole positions of ρ are determined for different Breit-Wigner parameterizations, which are (553 15 47) i(254 23 54) M eV= c^2 (constant width), (559 6 26) i(179 7 18) M eV= c^2 (width containing kinematic factor), (554 13 65) i(240 4 19) M eV= c^2 (P.K.U. ansatz), and (541 9 95) i(240 8 33) M eV= c^2 (Bugg & Zou's approach). The first Breit-Wigner parameterization may be problematic because the imaginary part does not vanish at threshold. The second parameterization gives a small width, and creates a virtual state in the real energy axis below the ρ threshold [29]. The final best esti-

mate of the ρ pole position from this analysis is $(552^{+84}_{-106}) - i(232^{+81}_{-72})$ M eV= c^2 , where the central values are obtained by a simple mean of the different Breit-Wigner parameterizations excluding the second one, while the errors cover the statistical and systematic errors, including the differences in the three Breit-Wigner parameterizations.

We also fit our data according to the scheme in Ref. [19]. It is found that the S -wave FSI plays a dominant role in $(2S) \rightarrow \pi^+ J/\psi$, while the contribution from the contact term is small. This means that the ρ meson has a significant contribution in this process. The ρ pole used in this fit, 469 i203 M eV/ c^2 is consistent with the fits to the Breit-Wigner functions. This implies that, although the two theoretical schemes are very different, both of them find the ρ meson at similar pole positions.

If the ρ meson exists, the pole should occur universally in all $\pi^+ J/\psi$ system with correct quantum numbers. Our analysis demonstrates that, in $(2S) \rightarrow \pi^+ J/\psi$, even though there is no apparent peak structure, one can still determine the pole location in good agreement with that obtained from $J/\psi \rightarrow \pi^+ \pi^-$ decay [17] by assuming a simple form of the contact term. Hence it provides further evidence for the ρ meson.

Acknowledgment

The BES collaboration thanks the staff of BEPC and computing center for their hard efforts. We are grateful to F.K. Guo and P.N. Shen for useful discussions and good suggestions. This work is supported in part by the National Natural Science Foundation of China under contracts Nos. 10491300, 10225524, 10225525, 10425523, the Chinese Academy of Sciences under contract No. KJ 95T-03, the 100 Talents Program of CAS under Contract Nos. U-11, U-24, U-25, and the Knowledge Innovation Project of CAS under Contract Nos. U-602, U-34 (IHEP), the National Natural Science Foundation of China under Contract No. 10225522 (Tsinghua University), and the Department of Energy under Contract No. DE-FG02-04ER41291 (U Hawaii).

REFERENCES

1. W. M. Yao et al. (Particle Data Group), *Journal of Physics G* 33 1 (2006). (URL: <http://pdg.lbl.gov>)
2. G. Abrams, *Proceedings of the 1975 International Symposium on Lepton and Photon Interactions at High Energies*, Published by the Stanford Linear Accelerator Center, 36 (1975).
3. J.Z. Bai et al., *Phys. Rev. D* 62 032002 (2000).
4. R.N. Cahn, *Phys. Rev. D* 12 3559 (1975).
5. J. Schwinger, *Ann. Phys.* 2 407 (1957);
M. Gell-Mann and M. Levy, *Nuovo Cim.* 16 705 (1960).
6. M. Taketani et al., *Prog. Theor. Phys. Suppl.* No.39 (1967); No.42 (1968).
7. N.A. Tomqvist and M. Roos, *Phys. Rev. Lett.* 76 1575 (1996);
R. Delbourgo and M.D. Scadron, *Phys. Rev. Lett.* 48 379 (1982).
8. J.E. Augustin, et al., *Nucl. Phys. B* 320 1 (1989).
9. N.Wu, BES Collaboration, in: *Proceedings of the XXXV Ith Rencontres de Moriond, Les Arcs, France, 17-24 March, 2001*.
10. D. A. Klei et al., *Phys. Lett. B* 397 350 (1997).
11. T. Ishida et al., in: *Proceedings of International Conference Hadron95, World Scientific, Manchester, UK, 1995*.
12. A summary of the related literatures before 1999 can be found in: V.E. Markushin, M.P. Locher, *Frascati Phys. Ser.* 15 229 (1999).
13. Z. Xiao and H.Q. Zheng, *Nucl. Phys. A* 695 273 (2001).
14. G. Colangelo, J. Gasser and H. Leutwyler, *Nucl. Phys. B* 603 125 (2001).
15. Z.Y. Zhou et al., *JHEP* 0502 043 (2005).
16. E.M. Aitala et al., *Phys. Rev. Lett.* 86 770 (2001).
17. M. Ablikim et al., *Phys. Lett. B* 598 149 (2004).
18. M. Ishida, *Prog. Theor. Phys. Suppl.* 149 190 (2003).
19. F.K. Guo et al., *Nucl. Phys. A* 761 269 (2005).
20. J.A. Oller and E. Oset, *Nucl. Phys. A* 620 438 (1997); (Erratum) *ibid.* 652 407 (1999).
21. F.K. Guo, P.N. Shen and H.C. Chiang, *Phys. Rev. D* 74 014011 (2006).
22. M. Xiao-hu et al., *HEP & NP* 28 (5) 455 (2004) (in Chinese).
23. J.Z. Bai et al., *Nucl. Instr. Meth. A* 344 (1994) 319 and A 458 627 (2001).
24. J. Z. Bai et al., *Phys. Rev. D* 58 092006 (1998).
25. M. Ablikim et al., *Nucl. Instrum. Meth. A* 552 344 (2005).
26. L.S. Brown and Robert N. Cahn, *Phys. Rev. Lett.* 35 1 (1975).
27. N.W.U et al., *Commun. Theor. Phys.* 35 547 (2001).
28. N.W.U et al., *Commun. Theor. Phys.* 37 309 (2002).
29. H.Q. Zheng et al., *Nucl. Phys. A* 733 235 (2004).
30. B.S. Zou and D.V. Bugg, *Euro. Phys. J A* 16 537 (2003).
31. F. James, CERN Program Library Long Writeup D 506.